SIAM J. IMAGING SCIENCES
Vol. 10, No. 2, pp. 535–557

Analytic Inversion of a Conical Radon Transform Arising in Application of Compton Cameras on the Cylinder*

Sunghwan Moon† and Markus Haltmeier‡

Abstract. Single photon emission computed tomography (SPECT) is a well-established clinical tool for functional imaging. A limitation of current SPECT systems is the use of mechanical collimation, where only a small fraction of the emitted photons are actually used for image reconstruction. This results in a large noise level and finally in a limited spatial resolution. In order to decrease the noise level and to increase the imaging resolution, Compton cameras have been proposed as an alternative to mechanical collimators. Image reconstruction in SPECT with Compton cameras yields the problem of recovering a marker distribution from integrals over conical surfaces. Due to this and other applications, such conical Radon transforms recently got significant attention. In the current paper we consider the case where the cones of integration have vertices on a circular cylinder and axis pointing to the symmetry axis of the cylinder. Our setup does not use all emitted photons but a much larger fraction than systems based on mechanical collimation. Further, it may be simpler to be fabricated than a Compton camera system collecting full five-dimensional data. As main theoretical results in this paper we derive analytic reconstruction methods for the considered transform. We also investigate the V-line transform with vertices on a circle and symmetry axis orthogonal to the circle, which arises in the special case where the absorber distribution is located in a horizontal plane.

Key words. conical Radon transform, nuclear imaging, Compton cameras, SPECT, image reconstruction, inversion formula

AMS subject classifications. 44A12, 65R10, 92C55

DOI. 10.1137/16M1083116

1. Introduction.

In this paper we study the inversion of a conical Radon transform that maps a function defined in three-dimensional space to its integrals over a special family of cones. Recovering a function from integrals over cones arises in single photon emission computed tomography (SPECT) using Compton cameras. These type measurement devices have been introduced as an alternative to classical gamma cameras (based on mechanical collimators) offering increased sensitivity [8, 18, 26, 31]. Inversion of conical Radon transforms is also relevant for single scattering optical tomography [9] or Compton scattering imaging [20]. Recently, various versions of conical Radon transforms have been studied (see, for example, [1, 4, 7, 11, 12, 15, 19, 20, 25, 27, 28, 30] and the references therein). The instance of

*Received by the editors July 5, 2016; accepted for publication (in revised form) December 28, 2016; published electronically April 13, 2017.
http://www.siam.org/journals/siims/10-2/M108311.html
Funding: The work of the first author was supported by the National Research Foundation of Korea grant funded by the Korea government (MSIP) (2015R1C1A1A01051674) and the TJ Park Science Fellowship of POSCO TJ Park Foundation.
†Department of Mathematical Sciences, Ulsan National Institute of Science and Technology, Ulsan 44919, Republic of Korea (shmoon@unist.ac.kr).
‡Department of Mathematics, University of Innsbruck, A-6020 Innsbruck, Austria (markus.haltmeier@uibk.ac.at).

the conical Radon transform that we study in this paper arises in the application of SPECT using certain types of cylindrical Compton cameras.

1.1. Compton cameras in SPECT. In SPECT, weakly radioactive tracers are given to the patient and participate in physiological processes. The radioactive tracers can be detected through the emission of gamma ray photons allowing one to infer information about physiological processes. In order to obtain sufficient location information about the emitted photons, the standard approach in SPECT is to use collimators which only record photons that enter the detector surface vertically. As illustrated in the left image in Figure 1, such data provide integrals of the tracer distribution over straight lines, and reconstructing the tracer distribution can be performed by inverting the (attenuated) X-ray transform [33]. A main drawback of the use of mechanical collimators is that they remove most photons, and therefore the number of recorded photons is low. To increase the sensitivity, the use of Compton cameras has been proposed in [8, 26, 31]. Opposed to classical gamma cameras, Compton cameras use two detector arrays in order to avoid the use of a mechanical collimator.

As illustrated in the right image in Figure 1, a Compton camera consists of a scatter detector array D_s and an absorption detector array D_a. A photon emitted in the direction of the camera undergoes Compton scattering in D_s, and is absorbed in D_a. In each detector, the position and the energy of the photon are measured [26]. The measured energies can be used to determine the scattering angle or half-opening angle ψ at D_s via the Compton scattering formula $\cos(\psi) = 1 - mc^2(E_s - E_a)/(E_sE_a)$, where m is the electron mass, c the speed of

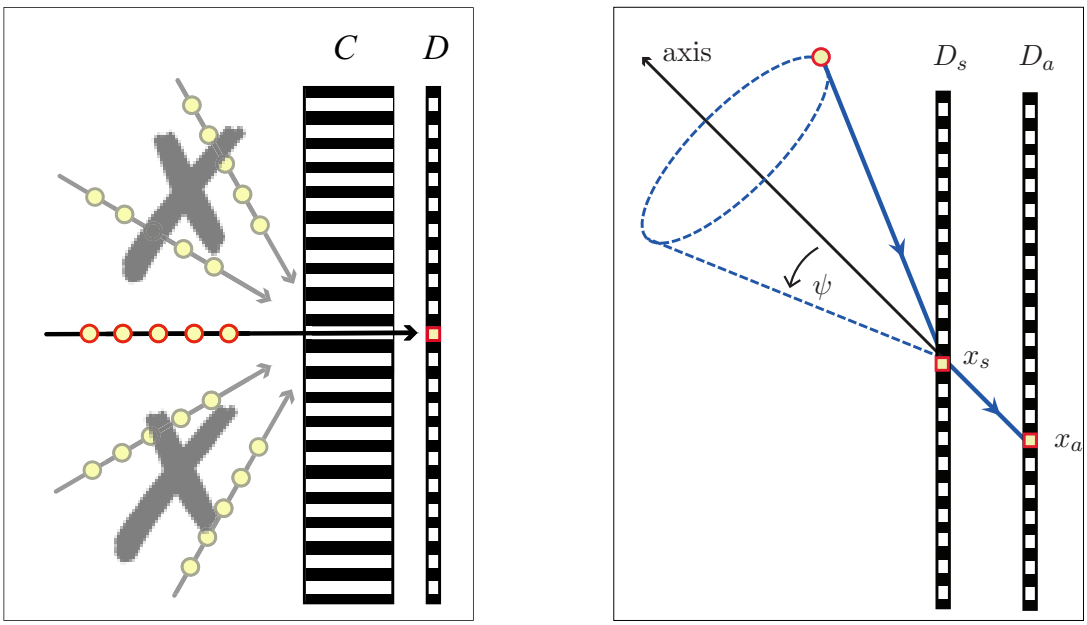

Figure 1. *Collimator versus Compton camera. Left: In standard gamma cameras, a collimator C is inserted, which lets pass only photons propagating orthogonal to the detector plane. The location of any emitted photon can be traced back to a straight line. Right: A Compton camera consists of two detector arrays D_s and D_a. Every observed photon can be traced back to the surface of a cone.*

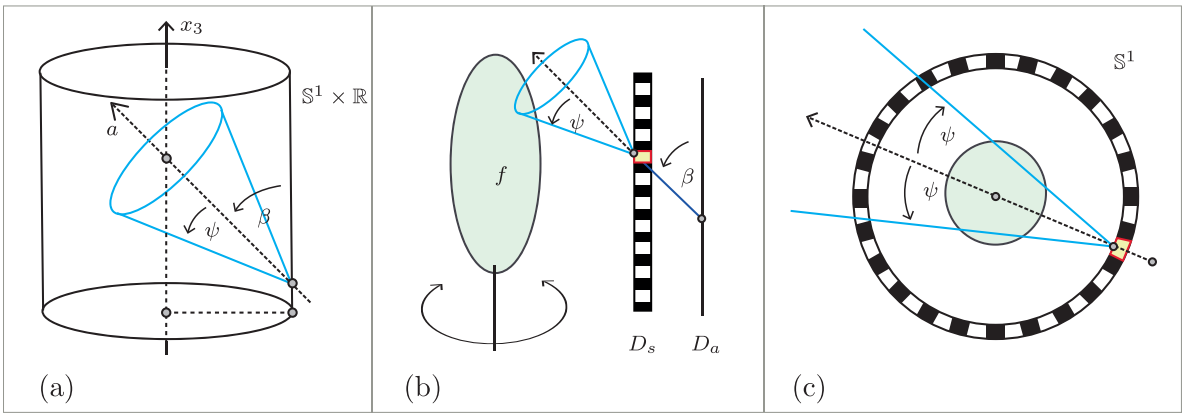

Figure 2. *Conical Radon transform on the cylinder.* (a) *The conical Radon transform integrates a function over all cones with the vertex on* $\mathbb{S}^1 \times \mathbb{R}$ *and the axis intersecting* $\{(0,0)\} \times \mathbb{R}$. (b) *Vertical cross section. The conical integrals may be obtained by rotating a one-dimensional Compton camera rotated around the* x_3*-axis.* (c) *Horizontal cross section. The conical integrals reduce to integrals over V-shaped line, with the vertex on* $\mathbb{S}^1$ *and the symmetry axis pointing to the origin.*

light, E_s the photon energy at D_s, and E_a the energy of the photon measured at D_a. Using this information, one can conclude that the observed photon must have been emitted on the surface of a circular cone, where the vertex is given by the position x_s at D_s, the central axis points from x_a (the position at D_a) to x_s, and the half-opening angle is given by ψ.

Now suppose we have given a distribution of tracers $f\colon \mathbb{R}^3 \to \mathbb{R}$ which emits photons uniformly in all directions. The expected number of photons recorded with data (x_s, E_s) and (x_a, E_a) is proportional to $K(\psi)I$, where I is the integral over the cone determined by (x_s, E_s) and (x_a, E_a) and $K(\psi)$ is the Klein–Nishina distribution which describes the probability that a given photon scatters by angle ψ. The Klein–Nishina distribution is known explicitly and is well-bounded from below for typical photon energies. After rescaling we can therefore assume that Compton cameras provide noisy versions of I, from which the tracer distribution f has to be recovered.

1.2. The conical Radon transform on the cylinder.

In this work we consider the situation where the scattering detector forms a cylindrical surface $\mathbb{S}^1 \times \mathbb{R}$ and that the source distribution f is assumed to be supported inside this cylinder. We assume that the available data consist of integrals over all cones with the vertex on $\mathbb{S}^1 \times \mathbb{R}$ and the central axis pointing to $\{(0,0)\} \times \mathbb{R}$; see Figure 2(a). Our goal is to recover f from its conical Radon transform, consisting of integrals of f over these cones. One possible way to realize a cylindrical Compton camera is illustrated in Figure 2(b), where, in a first step, data are collected with a one-dimensional Compton camera [3, 16]. Such a one-dimensional Compton camera consists of two linear detector arrays and records integrals over cones with the axis intersecting both linear detectors. In order to obtain the considered data, the one-dimensional Compton camera is rotated around the x_3-axis. In [16] it has been shown that data of a one-dimensional Compton camera without rotation is theoretically sufficient to recover the absorber distribution provided it is supported on one side of the plane joining the two linear detector arrays.

While f has a 3-dimensional domain, the class of cones we consider depends on four variables, and so we are facing an overdetermined inverse problem. Due to low photon counts

the use of such overdeterminated data is actually a desired feature of Compton cameras (see, for example, the discussion in [1]). Standard image reconstruction approaches for Compton camera imaging even use integrals over a five-dimensional set of conical integrals. Our data consist of a four-dimensional subset of the data and, in particular, again do not use all emitted photons. However, collecting full five-dimensional data requires advanced electronic wiring between the absorption and the scattering detectors for performing the necessary coincidence measurements. It can therefore be seen as practical benefit of our work that we only require a subset of all conical integrals, which can be realized by simpler electronic wiring between the absorption and the scattering detectors.

Additionally, we consider a special two-dimensional version of the conical Radon transform. Suppose that the support of the phantom is thin and contained in a horizontal plane, such that we can model it by $f(x_1, x_2, x_3) = \delta(x_3)F(x_1, x_2)$, where δ is the one-dimensional delta distribution. In such a situation it is reasonable to restrict the set of vertices to $\mathbb{S}^1 \times \{0\}$. The intersection of any corresponding cone with the plane $\{x \in \mathbb{R}^3 \mid x_3 = 0\}$ becomes a V-line with the vertex on $\mathbb{S}^1$ and the axis pointing to the origin; see Figure 2(c). Reconstructing the function F from the resulting V-line transform will be considered in section 2. In fact the developed inversion method for the V-line transform is the basis of one of our inversion methods for the three-dimensional conical Radon transform. Another interesting two-dimensional case would arise when f is restricted to a vertical plane and the vertices of the cones are located on a line pointing in the x_3-direction. The resulting V-line transform with vertices on a line has been studied in previous works, such as [1, 3, 12, 15, 19, 32], and therefore will not be investigated in the present work.

1.3. Outline. This manuscript is organized as follows. In section 2 we define the V-line transform with vertices on the circle and derive an explicit inversion formula based on a Fourier series expansion. This, in particular, implies the invertibility of the V-line transform. In section 3 we present two inversion methods for inverting the conical Radon transform with vertices on the cylinder and the axis pointing to the symmetry axis of the cylinder. The first method even works when a radial weight is included in the conical Radon transform and is based on reducing the conical Radon transform to the V-line transform. The second method uses an approach of Smith [27] and reduces the conical Radon transform to the standard Radon transform. We use this technique to derive explicit inversion formulas and further derive Sobolev stability estimates for inverting the conical Radon transform. Generalizations of our results to higher dimension are presented in the appendix.

2. V-line transform with vertices on a circle.

In this section we study the V-line transform on the circle. We derive an explicit inversion formula using a Fourier series expansion, which, in particular, implies the invertibility of the V-line transform, and further derive a numerical reconstruction algorithm based on our inversion formula.

2.1. Explicit inversion formula. For $\varphi \in [0, 2\pi)$ we write $\theta(\varphi) := (\cos\varphi, \sin\varphi)$. Further, we denote by $D_1(0) := \{x \in \mathbb{R}^2 \mid \|x\| < 1\}$ the unit disc in $\mathbb{R}^2$ and by $C_c^\infty(D_1(0))$ the set of all C^∞-functions $F\colon \mathbb{R}^2 \to \mathbb{R}$ with $\operatorname{supp}(F) \subseteq D_1(0)$.

Definition 2.1 (the V-line transform on the circle). *Let $F \in C_c^\infty(D_1(0))$. We define the* V-line transform *of F by*

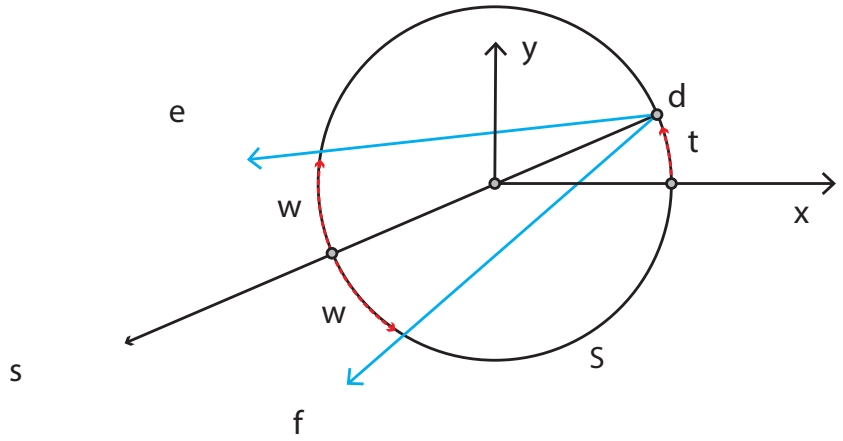

Figure 3. *The V-line transform on the circle. The V-line transform on the circle integrates a function supported in the disc over V-lines with vertex* $\theta(\varphi) = (\cos\varphi, \sin\varphi)$*, symmetry axis* $\{(1-r)\,\theta(\varphi) \mid r > 0\}$*, and half-opening angle* ψ*.*

$$\mathcal{V}F\colon [0,2\pi) \times (0,\pi/2) \to \mathbb{R}\colon (\varphi,\psi) \mapsto \sum_{\sigma=\pm 1} \int_0^\infty F(\theta(\varphi) - r\theta(\varphi - \sigma\psi))\,\mathrm{d}r\,. \tag{2.1}$$

As illustrated in Figure 3, the V-line transform integrates the function F over V-lines (one-sided cones in the plane), having the vertex $\theta(\varphi) := (\cos\varphi, \sin\varphi) \in \mathbb{S}^1$, symmetry axis $\{(1-r)\,\theta(\varphi) \mid r > 0\}$, and half-opening angle ψ. In the following we will frequently make use of the two-dimensional (regular) Radon transform of a function $F \in C_c^\infty(\mathbb{R}^2)$, defined by

$$(\mathcal{R}F)(\alpha, s) := \int_{\mathbb{R}} F\left(s\cos(\alpha) - t\sin(\alpha), s\sin(\alpha) + t\cos(\alpha)\right) \mathrm{d}t \quad \text{for } (\alpha, s) \in [0, 2\pi) \times \mathbb{R}\,.$$

The Radon transform integrates the function F over the line $\{x \in \mathbb{R}^2 \mid (\cos(\alpha), \sin(\alpha)) \bullet x = s\}$ having a normal vector $(\cos(\alpha), \sin(\alpha))$ and an oriented distance $s \in \mathbb{R}$ from the origin.

The inversion approach we present below uses the Fourier series of F and $\mathcal{V}F$ with respect to the angular variables,

$$F\left(r\theta(\varphi)\right) = \sum_{n\in\mathbb{Z}} F_n(r)\, e^{in\varphi} \qquad \text{with} \quad F_n(r) := \frac{1}{2\pi}\int_0^{2\pi} F(r\theta(\varphi))\, e^{-in\varphi}\mathrm{d}\varphi\,, \tag{2.2}$$

$$(\mathcal{V}F)(\varphi,\psi) = \sum_{n\in\mathbb{Z}} (\mathcal{V}F)_n(\psi)\, e^{in\varphi} \quad \text{with} \quad (\mathcal{V}F)_n(\psi) := \frac{1}{2\pi}\int_0^{2\pi} (\mathcal{V}F)(\varphi,\psi)\, e^{-in\varphi}\mathrm{d}\varphi\,. \tag{2.3}$$

For $k \geq 0$, we denote by $T_k(z)$ and $U_k(z)$ the Chebyshev polynomials of the first and second kinds, respectively, where

$$T_k(z) := \begin{cases} \cos\left(k \arccos(z)\right) & \text{for } |z| \leq 1, \\ \cosh(k \operatorname{arccosh}(z)) & \text{for } z > 1, \\ (-1)^k \cosh(k \operatorname{arccosh}(-z)) & \text{for } z < -1, \end{cases}$$

$$U_k(z) := \begin{cases} \sin((k+1)\arccos(z))/\sin(\arccos(z)) & \text{for } |z| \le 1, \\ \sinh((k+1)\operatorname{arccosh}(z))/\sinh(\operatorname{arccosh}(z)) & \text{for } z > 1, \\ (-1)^k \sinh((k+1)\operatorname{arccosh}(-z))/\sinh(\operatorname{arccosh}(-z)) & \text{for } z < -1\,, \end{cases}$$

and set $U_{-1} := 0$.

Our strategy for inverting $\mathcal{V}$ is to recover the Fourier coefficient F_n from $(\mathcal{V}F)_n$ for any $n \in \mathbb{Z}$. For that purpose we proceed by setting up a one-dimensional integral equation for F_n in terms of $(\mathcal{R}F)_n$ that will subsequently be solved explicitly.

Lemma 2.2 (expressing $(\mathcal{V}F)_n$ in terms of F_n). *Suppose $F \in C_c^\infty(D_1(0))$ and let F_n and $(\mathcal{V}F)_n$ denote the Fourier coefficients of F and $\mathcal{V}F$ as defined in (2.2) and (2.3), respectively. Then, for all $(n, \psi) \in \mathbb{Z} \times (0, \pi/2)$, we have*

$$(\mathcal{V}F)_n(\psi) = 4\cos(n(\psi - \pi/2)) \int_{\sin(\psi)}^1 F_n(r) \frac{r\, T_{|n|}(\sin(\psi)/r)}{\sqrt{r^2 - \sin^2(\psi)}} \mathrm{d}r\,. \tag{2.4}$$

Proof. From the definitions of $\mathcal{V}F$ and $\mathcal{R}F$ we have the following relation

$$\mathcal{V}F(\varphi, \psi) = \mathcal{R}F(\varphi - \psi + \pi/2, \sin(\psi)) + \mathcal{R}F(\varphi + \psi - \pi/2, \sin(\psi))\,. \tag{2.5}$$

Now let $(\mathcal{R}F)_n(s) := \frac{1}{2\pi}\int_0^{2\pi} (\mathcal{R}F)(\alpha, s)\, e^{-in\alpha} \mathrm{d}\alpha$ denote the nth Fourier coefficient of $\mathcal{R}F$ with respect to the angular variable. Equation (2.5), the definition of the Fourier coefficients of $\mathcal{V}F$ and $\mathcal{R}F$, and two variable substitutions yield

$$\begin{aligned} &(\mathcal{V}F)_n(\psi) \\ &= \frac{1}{2\pi}\int_0^{2\pi} \left[\mathcal{R}F(\varphi - \psi + \pi/2, \sin(\psi)) + \mathcal{R}F(\varphi + \psi - \pi/2, \sin(\psi))\right] e^{-in\varphi} \mathrm{d}\varphi \\ &= \frac{1}{2\pi}\int_0^{2\pi} \mathcal{R}F(\alpha, \sin(\psi))\, e^{-in(\alpha + \psi - \pi/2)} \mathrm{d}\alpha + \frac{1}{2\pi}\int_0^{2\pi} \mathcal{R}F(\alpha, \sin(\psi))\, e^{-in(\alpha - \psi + \pi/2)} \mathrm{d}\alpha \\ &= (\mathcal{R}F)_n(\sin(\psi))\, e^{-in(\psi - \pi/2)} + (\mathcal{R}F)_n(\sin(\psi))\, e^{in(\psi - \pi/2)} \\ &= 2\cos(n(\psi - \pi/2))\, (\mathcal{R}F)_n(\sin(\psi))\,. \end{aligned} \tag{2.6}$$

Next we note the relation $(\mathcal{R}F)_n(s) = 2\int_s^1 F_n(r) \frac{r\, T_{|n|}(s/r)}{\sqrt{r^2 - s^2}} \mathrm{d}r$ that was first derived by Cormack in [5]. Combining this with the last displayed equation yields (2.4). ∎

Lemma 2.2 together with known inversion formulas for the Radon transform yields the following explicit inversion formulas for the V-line transform on the circle.

Theorem 2.3 (inversion of the V-line transform on the circle). *Suppose $F \in C^\infty(D_1(0))$ and let F_n and $(\mathcal{V}F)_n$ denote the Fourier coefficients of F and $\mathcal{V}F$, as defined in (2.2) and (2.3). Then the following inversion formulas hold:*

$$F_n(r) = -\frac{1}{2\pi}\int_r^1 \frac{\partial}{\partial s}\left[\frac{(\mathcal{V}F)_n(\arcsin(s))}{\cos(n(\arcsin(s) - \pi/2))}\right] \frac{T_{|n|}(s/r)}{\sqrt{s^2 - r^2}}\, \mathrm{d}s\,, \tag{2.7}$$

$$F_n(r) = -\frac{1}{2\pi r}\left\{\int_r^1 \frac{\partial}{\partial s}\left[\frac{(\mathcal{V}F)_n(\arcsin(s))}{\cos(n(\arcsin(s)-\pi/2))}\right]\frac{\left[s/r+\sqrt{s^2/r^2-1}\right]^{-|n|}}{\sqrt{s^2/r^2-1}}\,\mathrm{d}s - \int_0^r \frac{\partial}{\partial s}\left[\frac{(\mathcal{V}F)_n(\arcsin(s))}{\cos(n(\arcsin(s)-\pi/2))}\right]U_{|n|-1}(s/r)\,\mathrm{d}s\right\}. \tag{2.8}$$

Proof. Let $(\mathcal{R}F)_n$ denote the nth Fourier coefficient of $\mathcal{R}F$. Then (2.6) implies

$$(\mathcal{R}F)_n(s) = \frac{(\mathcal{V}F)_n(\arcsin(s))}{2\cos(n(\arcsin(s)-\pi/2))}. \tag{2.9}$$

Next we recall the following inversion formulas for the Radon transform:

$$F_n(r) = -\frac{1}{\pi}\int_r^1 \frac{\partial(\mathcal{R}F)_n(s)}{\partial s}\frac{T_{|n|}(s/r)}{\sqrt{s^2-r^2}}\,\mathrm{d}s, \tag{2.10}$$

$$F_n(r) = -\frac{1}{\pi r}\left\{\int_r^1 \frac{\partial(\mathcal{R}F)_n(s)}{\partial s}\frac{\left[s/r+\sqrt{s^2/r^2-1}\right]^{-|n|}}{\sqrt{s^2/r^2-1}}\,\mathrm{d}s - \int_0^r \frac{\partial(\mathcal{R}F)_n(s)}{\partial s}U_{|n|-1}(s/r)\,\mathrm{d}s\right\}. \tag{2.11}$$

Here (2.10) is Cormack's inversion formula [5] and (2.11) an inversion formula with better stability properties first derived in [24]. Inserting (2.9) into (2.10) yields the inversion formula (2.7), whereas inserting (2.11) yields (2.8). ∎

Theorem 2.3 in particular implies that the V-line transform is uniquely invertible. Further, it implies the following inversion method for the V-line transform.

Algorithm 2.4 (inversion of the V-line transform).
- Step 1: *Compute the Fourier coefficients* $(\mathcal{V}F)_n$ *of* $\mathcal{V}F$*; see* (2.3).
- Step 2: *Recover the Fourier coefficients* F_n *from* $(\mathcal{V}F)_n$ *by* (2.7) *or* (2.8).
- Step 3: *Recover* F *from its Fourier coefficients* F_n*; see* (2.2).

The inversion formula (2.7) solves the exterior problem for the V-line transform, because for reconstructing $F_n(r)$ it only uses integrals over V-lines that do not intersect the disc $\{x \in \mathbb{R}^2 \mid |x| \le r\}$. Such data can be stably obtained from exterior data of the Radon transform. As a consequence, evaluating (2.7) is numerically unstable (severely ill-posed). Note that the apparent divergence in (2.7), first solved in [24], has later also been resolved by Cormack in [6]. For the following, we therefore only consider the inversion formula (2.8) and we demonstrate that it can be evaluated stably and efficiently.

2.2. Numerical implementation. In this subsection we describe how to numerically implement Algorithm 2.4. In our implementation, we discretize any step in Algorithm 2.4. For computing the Fourier coefficients in Step 1 and for evaluating the Fourier series in Step 3, we use the standard FFT algorithm. For Step 1, the FFT algorithm outputs approximations $\mathrm{G}[n,j] \simeq (\mathcal{V}F)_n(\arcsin(s_j))$ for $n \in \{-N/2, -N/2+1, \ldots, N/2-1\}$ and $j \in \{0, \ldots, M\}$.

The main issue in the reconstruction procedure is implementing the inversion formula (2.8) in Step 2. Consider equidistant grid points $r_i = i/M$ for $i \in \{0, \dots, M\}$ and rewrite the inversion formula (2.8) in the form

$$F_n(r) = \frac{1}{\pi}\left\{ \int_0^r g_n'(s) U_{|n|-1}(s/r)\, \frac{\mathrm{d}s}{r} - \int_r^1 g_n'(s) \frac{\left[s/r + \sqrt{s^2/r^2 - 1}\,\right]^{-|n|}}{\sqrt{s^2/r^2 - 1}}\, \frac{\mathrm{d}s}{r} \right\},$$
$$g_n'(s) := \frac{\partial}{\partial s}\left[\frac{(\mathcal{V}F)_n(\arcsin(s))}{2\cos(n(\arcsin(s) - \pi/2))} \right].$$

These formulas are used for finding approximations to $F_n(r_i)$ as follows. First, for some small regularization parameter $\epsilon > 0$ (that accounts for instabilities due to the zeros in the denominator in the definition to g_n') we define

$$\mathrm{H}[n,j] := \frac{\cos(n(\arcsin(s_j) - \pi/2))\, \mathrm{G}[n,j]}{\epsilon^2 + \cos(n(\arcsin(s_j) - \pi/2))^2}, \tag{2.12}$$

and take $g_n'[j] := (\mathrm{H}[n, j+1] - \mathrm{H}[n,j])/(2M)$ as an approximation of $g_n'(s)$ on the interval $[r_j, r_{j+1}]$. Using such an approximation, we obtain

$$\begin{aligned}
F_n(r_i) &= \frac{1}{\pi}\left\{ \int_0^{r_i} g_n'(s) U_{|n|-1}(s/r_i)\, \frac{\mathrm{d}s}{r_i} - \int_{r_i}^1 g_n'(s) \frac{\left[s/r_i + \sqrt{s^2/r_i^2 - 1}\,\right]^{-|n|}}{\sqrt{s^2/r_i^2 - 1}}\, \frac{\mathrm{d}s}{r_i} \right\} \\
&= \frac{1}{\pi}\left\{ \sum_{j=0}^{i-1} \int_{r_j}^{r_{j+1}} g_n'(s) U_{|n|-1}(s/r_i)\, \frac{\mathrm{d}s}{r_i} \right. \\
&\qquad \left. - \sum_{j=i}^{M-1} \int_{r_j}^{r_{j+1}} g_n'(s) \frac{\left[s/r_i + \sqrt{s^2/r_i^2 - 1}\,\right]^{-|n|}}{\sqrt{s^2/r_i^2 - 1}}\, \frac{\mathrm{d}s}{r_i} \right\} \\
&\simeq \frac{1}{\pi}\left\{ \sum_{j=0}^{i-1} g_n'[j] \int_{r_j}^{r_{j+1}} U_{|n|-1}(s/r_i)\, \frac{\mathrm{d}s}{r_i} \right. \\
&\qquad \left. - \sum_{j=i}^{M-1} g_n'[j] \int_{r_j}^{r_{j+1}} \frac{\left[s/r_i + \sqrt{s^2/r_i^2 - 1}\,\right]^{-|n|}}{\sqrt{s^2/r_i^2 - 1}}\, \frac{\mathrm{d}s}{r_i} \right\}.
\end{aligned}$$

By elementary integration one verifies that

$$\forall j \in \{0, \dots, i-1\}: \quad w_{i,j}^{(n)} := \int_{r_j}^{r_{j+1}} U_{|n|-1}(s/r_i)\, \frac{\mathrm{d}s}{r_i} \tag{2.13}$$
$$= \begin{cases} 0 & \text{for } n = 0, \\ \dfrac{1}{|n|}\left(T_{|n|}(r_{j+1}/r_i) - T_{|n|}(r_j/r_i)\right) & \text{for } n \neq 0, \end{cases}$$

and

$$(2.14)\quad \forall j \in \{i,\dots,M-1\}: \quad w_{i,j}^{(n)} := \int_{r_j}^{r_{j+1}} -\frac{\left[s/r_i + \sqrt{s^2/r_i^2-1}\,\right]^{-|n|}}{\sqrt{s^2/r_i^2-1}}\,\frac{\mathrm{d}s}{r_i}$$
$$= \begin{cases} -\log\left(r_{j+1}+\sqrt{r_{j+1}^2-r_i^2}\right)\log\left(r_j+\sqrt{r_j^2-r_i^2}\right) & \text{for } n=0,\\ -\dfrac{1}{|n|}\left(e^{-|n|\,\operatorname{arccosh}(r_{j+1}/r_i)}-e^{-|n|\,\operatorname{arccosh}(r_j/r_i)}\right) & \text{for } n\neq 0\,. \end{cases}$$

Consequently, we obtain

$$(2.15)\quad \forall (n,i)\in\{-N/2,\dots,N/2-1\}\times\{1,\dots,M\}: \quad \mathrm{F}[n,i] = \sum_{j=0}^{M-1} w_{i,j}^{(n)}\,\frac{\mathrm{H}[n,j]-\mathrm{H}[n,j]}{2\pi M},$$

where $\mathrm{H}[n,j]$ is given by (2.12), the weights $w_{i,j}^{(n)}$ are defined by (2.13) and (2.14), and $\mathrm{F}[n,i]$ is the desired approximation to $F_n(r_i)$.

Formula (2.15) immediately yields the following discrete reconstruction algorithm for inverting the V-line transform using discrete data.

Algorithm 2.5 (discrete reconstruction algorithm for inverting the V-line transform).
- Step 1: *Use the FFT to compute the* $\mathrm{G}[n,i] \simeq (\mathcal{V}F)_n(s_i)$.
- Step 2: *For some* $\epsilon > 0$, *compute* $\mathrm{H}[n,i] \simeq (\mathcal{R}F)_n(s_i)$ *by evaluating* (2.12).
- Step 3: *Compute* $\mathrm{F}[n,i] \simeq F_n(r_i)$ *by evaluating* (2.15).
- Step 4: *Approximate* $F(r_i\cos\varphi_k, r_i\cos\varphi_k)$ *by applying the inverse FFT algorithm.*

Algorithm 2.5 is numerically efficient in the following sense. If $M=\mathcal{O}(N)$, easy arguments show that the proposed algorithm only requires $\mathcal{O}(N^3)$ floating point operations for reconstructing the phantom at N^2 reconstruction points. This is the same complexity as filtered backprojection reconstruction algorithms have. Notice further that by evaluating (2.15) in Step 3 in Algorithm 2.5 we actually implement the inversion formula (2.11) for the regular Radon transform derived by Perry [24]. The proposed implementation of (2.11) is of interest on its own and is different from the implementation given in [13]. Finally note that a different reconstruction strategy based on (2.12) (or (2.9)) would be to first recover $\mathcal{R}F$ by applying the inverse FFT algorithm and then to apply any existing reconstruction algorithm for the Radon transform such as the filtered backprojection algorithm.

2.3. Numerical examples. The reconstruction procedure outlined above has been implemented in MATLAB and tested on a discretized version of a Smiley phantom shown in Figure 4(a) sampled on a Cartesian 201×201 grid. For implementing the V-line transform we first numerically computed the X-ray transform $\mathcal{X}F(\varphi,\psi) = \int_0^\infty F(\theta(\varphi)-r(\cos(\varphi-\psi),\sin(\varphi-\psi)))\mathrm{d}r$ by computing the ray integrals using the composite trapezoidal rule. We then evaluated the V-line transform using $\mathcal{V}F(\varphi,\psi) = \sum_{\sigma=\pm1}\mathcal{X}F(\varphi,\sigma\psi)$. Figures 4(b) and (c) show the numerically computed V-line and X-ray transforms for $m=256$ vertex positions and $N=201$ opening angles in the interval $[0,\pi/2]$.

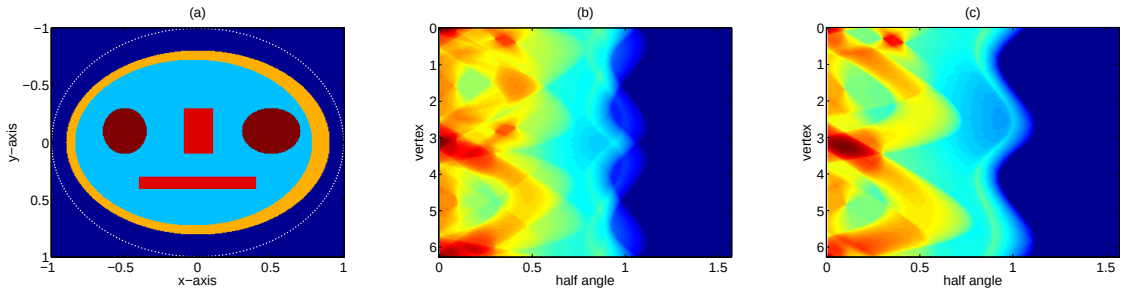

Figure 4. (a) *Phantom F used for numerical simulations.* (b) *Corresponding V-line transform $\mathcal{V}F$.* (c) *Corresponding X-ray transform $\mathcal{X}F$.*

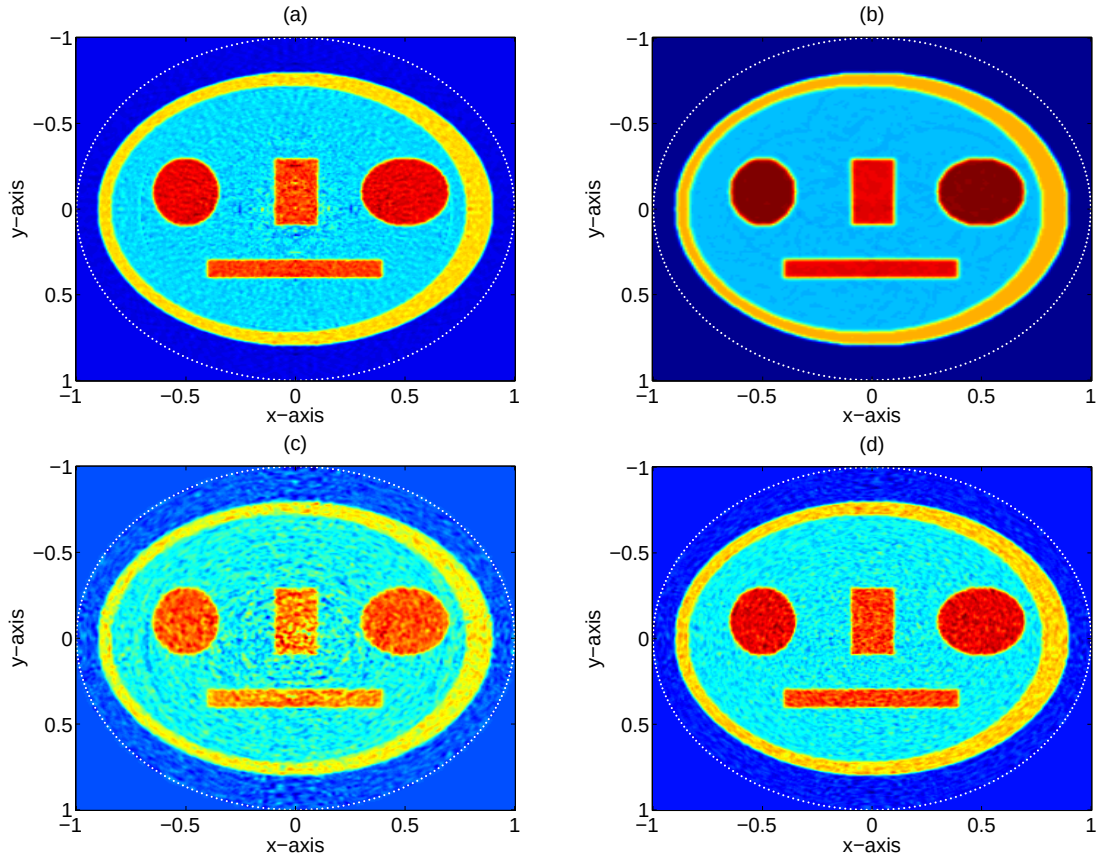

Figure 5. (a) *Reconstruction from numerically computed V-line transform.* (b) *Reconstruction from numerically computed X-ray transform.* (c) *Reconstruction from V-line transform after adding Gaussian white noise to the data.* (d) *Reconstruction from X-ray transform after adding Gaussian white noise to the data.*

The numerical reconstruction from the V-line transform using Algorithm 2.5 evaluated on a Cartesian 201×201 grid is shown in Figure 5(a). The regularization parameter has been taken as $\epsilon = 0.005$. For comparison purposes we also applied our reconstruction algorithm to the X-ray transform; see Figure 5(b). For inverting the X-ray transform, (2.12) is replaced

by $\mathrm{H}[n,j] := \mathrm{G}[n,j]/\exp(-in(\arcsin(s_j)-\pi/2))$. (In fact, such a reconstruction procedure is justified by (2.5) and (2.6).) Because $\exp(-int) \neq 0$, no regularization is necessary for inverting $\mathcal{X}F$. Finally, in order to demonstrate the stability of our algorithm we added 5% noise to the data and repeated the computations. For inverting the V-line transform we used an increased regularization parameter equal to $\epsilon = 0.05$. Again the results for both the V-line and the X-ray transforms are quite good. However, the inversion of the V-line transform is slightly more sensitive to the noise which is expected due to the zeros of the function $s \mapsto \cos(n(\arcsin(s)-\pi/2))$ appearing in the denominator of the inversion formula for $\mathcal{V}F$.

3. The conical Radon transform with vertices on a cylinder.

In this section we study the inversion of the conical Radon transform on the cylinder using four-dimensional data. For that purpose, for $(\varphi, z, \beta, \psi) \in [0, 2\pi) \times \mathbb{R} \times (0,\pi)^2$, we use the following notations:

- $\theta(\varphi) := (\cos\varphi, \sin\varphi) \in \mathbb{S}^1$;
- $a(\varphi,\beta) := (-\theta(\varphi)\sin(\beta), \cos(\beta)) \in \mathbb{S}^2$;
- $C(\varphi,z,\beta,\psi) := (\theta(\varphi), z) + \{x \in \mathbb{R}^3 \mid a(\varphi,\beta)\bullet x = \|x\|\cos\psi\}$.

The set $C(\varphi,z,\beta,\psi)$ is a one-sided circular cone, having a vertex $(\theta(\varphi),z) \in \mathbb{S}^1\times\mathbb{R}$, a symmetry axis $(\theta(\phi),z) + \{ra(\varphi,\beta) \mid r > 0\}$ pointing to the symmetry axis of the cylinder $\mathbb{S}^1 \times \mathbb{R}$, and a half-opening angle $\psi \in (0,\pi)$; see Figure 2(a).

Definition 3.1 (conical Radon transform on the cylinder). *Let $k \in \mathbb{N}_0 = \{0, 1, \dots\}$ and $f \in C_c^\infty(D_1(0)\times\mathbb{R})$. We define the* (weighted) conical Radon transform *of f by*

$$\mathcal{C}_k f\colon [0,2\pi)\times\mathbb{R}\times(0,\pi)^2 \to \mathbb{R}\colon \tag{3.1}$$
$$(\varphi,z,\beta,\psi) \mapsto \int_{C(\varphi,z,\beta,\psi)} f(x)\,\|x-(\theta(\varphi),z)\|^{k-1}\,\mathrm{d}S(x)\,.$$

The weighted conical Radon transform maps the function f to integrals over members of the four-dimensional set of all cones $\{C(\varphi,z,\beta,\psi) \subseteq \mathbb{R}^3 \mid (\varphi,z,\beta,\psi) \in [0,2\pi)\times\mathbb{R}\times(0,\pi)^2\}$. The parameter $k \in \mathbb{N}_0$ allows us to include a radial weight that can be adjusted to a particular application at hand. In the literature on Compton camera imaging the cases $k = 0$ and $k = 1$ have been used. In [27], the case $k = 1$ is referred to as the surface integral model, and the case $k = 0$ as the cone-beam line integral model. Notice that the V-line transform studied in the previous section corresponds to the cone-beam line integral model, in the sense that $\mathcal{V}F(\varphi,\psi) = \mathcal{C}_0 f(\varphi,0,0,\psi)$ when $f(x_1,x_2,x_3) = \delta(x_3)F(x_1,x_2)$.

In the following we present two inversion methods for inverting $\mathcal{C}_k$. The first one is based on reducing the conical Radon transform to the V-line transform, whereas the second one is based on reducing the conical Radon transform to the Radon transform.

3.1. Method 1: Reduction to the V-line transform.

The first inversion method consists in first recovering the V-line transform from $\mathcal{C}_k f$ and subsequently recovering f by inverting the V-line transform. For that purpose we make use of the (weighted) X-ray transform

$$(\mathcal{X}_k f)\colon [0,2\pi)\times\mathbb{R}\times\mathbb{R}^3\setminus\{0\} \to \mathbb{R}\colon (\varphi,z,u) \mapsto \int_0^\infty f((\theta(\varphi),z)+ru))r^k\mathrm{d}r\,, \tag{3.2}$$

for $k \in \mathbb{N}_0$ and $f \in C_c^\infty(D_1(0)\times\mathbb{R})$. The X-ray transform consists of integrals over rays $\{(\theta(\varphi),z)+ru \mid r>0\}$ with a vertex $(\theta(\varphi),z) \in \mathbb{S}^1\times\mathbb{R}$ and a direction $u \in \mathbb{R}^3\setminus\{0\}$. Note

that we take the direction u in (3.2) as an arbitrary element in $\mathbb{R}^3$, because this is required for our proof of the following Lemma 3.2. In fact, Lemma 3.2 is one of the central results in this paper and allows us to reduce the conical Radon transform $\mathcal{C}_k$ to the V-line transform. It states that performing appropriate manipulations (differentiation and integrations) on the integrals $\mathcal{C}_k f(\varphi, z, \beta, \psi)$ over cones with a fixed vertex $(\theta(\varphi), z)$ yields the integral of f over a V-shaped line with vertex $(\theta(\varphi), z)$.

Lemma 3.2. *Let $f \in C_0^\infty(D_1(0) \times \mathbb{R})$ and $(\varphi, z) \in [0, 2\pi) \times \mathbb{R}$. For any $y = (y_1, y_2) \in \mathbb{R}^2$ with $\|y\| \leq 1$, we have*

$$\sum_{\sigma=\pm 1} (\mathcal{X}_k f)\left(\varphi, z, y_1\theta(\varphi) + \sigma\sqrt{1-\|y\|^2}\,\theta(\varphi)^\perp, y_2\right) = \frac{\sqrt{1-\|y\|^2}}{2\pi^2} \int_0^\pi \int_0^\pi \frac{\partial_\psi[\mathcal{C}_k f(\varphi, z, \beta, \psi)/\sin\psi]}{\cos(\psi) - y \bullet (-\sin(\beta), \cos(\beta))} \mathrm{d}\psi \mathrm{d}\beta\,. \tag{3.3}$$

Further, for any $k \geq 1$ and any $v \in \mathbb{S}^1$, we have

$$(\mathcal{X}_0 f)(\varphi, z, v, 0) = \frac{(-1)^{k-1}}{(k-1)!} \int_{-\pi/2}^0 \sin^{k-1}(\gamma)(\partial_z^k \mathcal{X}_k f)\left(\varphi, z, v\cos(\gamma), \sin(\gamma)\right) \mathrm{d}\gamma. \tag{3.4}$$

Proof. Using the one-dimensional delta distribution, we have

$$\begin{aligned}
\mathcal{C}_k f(\varphi, z, \beta, \psi) &= \sin(\psi) \int_{\mathbb{S}^2} \int_0^\infty f\left((\theta(\varphi), z) + r\omega\right) \delta\left(a(\varphi, \beta) \bullet \omega - \cos(\psi)\right) r^k \mathrm{d}r \mathrm{d}S(\omega) \\
&= \sin(\psi) \int_{\mathbb{S}^2} (\mathcal{X}_k f)(\varphi, z, \omega) \delta\left(a(\varphi, \beta) \bullet \omega - \cos(\psi)\right) \mathrm{d}S(\omega) \\
&= \sum_{\sigma=\pm 1} \sin(\psi) \int_{\mathbb{S}^2_\sigma} (\mathcal{X}_k f)(\varphi, z, \omega) \delta\left(a(\varphi, \beta) \bullet \omega - \cos(\psi)\right) \mathrm{d}S(\omega)\,, \qquad (3.5)
\end{aligned}$$

where $\mathbb{S}^2_\sigma := \{\omega \in \mathbb{S}^2 \mid (\sigma\theta(\varphi)^\perp, 0) \bullet \omega \geq 0\}$. Any element on the half-sphere $\mathbb{S}^2_\sigma$ can uniquely be written in the form $\omega = (y_1\theta(\varphi) + \sigma\sqrt{1-\|y\|^2}\theta(\varphi)^\perp, y_2)$ for $y = (y_1, y_2) \in \mathbb{R}^2$ with $\|y\| \leq 1$. Using this representation we have $a(\varphi, \beta) \bullet \omega = (-\sin(\beta), \cos(\beta)) \bullet y$. Together with (3.5) and the transformation rule this shows

$$\mathcal{C}_k f(\varphi, z, \beta, \psi) = \sum_{\sigma=\pm 1} \int_{\|y\|<1} (\mathcal{X}_k f)\left(\varphi, z, \left(y_1\theta(\varphi) + \sigma\sqrt{1-\|y\|^2}\theta(\varphi)^\perp, y_2\right)\right) \times \delta\left((-\sin(\beta), \cos(\beta)) \bullet y - \cos(\psi)\right) \frac{\sin(\psi)\mathrm{d}y}{\sqrt{1-\|y\|^2}}\,.$$

Now for fixed φ, z, and k, we define functions $F_\sigma \colon \mathbb{R}^2 \to \mathbb{R}$ by

$$F_\sigma(y) := \begin{cases} (\mathcal{X}_k f)\left(\varphi, z, y_1\theta(\varphi) + \sigma\sqrt{1-\|y\|^2}\,\theta(\varphi)^\perp, y_2\right) \dfrac{1}{\sqrt{1-\|y\|^2}} & \text{for } \|y\| \leq 1, \\ 0 & \text{for } \|y\| > 1, \end{cases}$$

and recall that the two-dimensional Radon transform can be written in the form $\mathcal{R}F(\alpha,s) = \int_{\mathbb{R}^2} F(y)\delta\left((\cos(\alpha),\sin(\alpha))\bullet y - s\right)\mathrm{d}y$; we will therefore obtain $\mathcal{C}_k f(\varphi,z,\beta,\psi)/\sin\psi = \sum_{\sigma=\pm1}(\mathcal{R}F_\sigma)(\beta+\pi/2,\cos(\psi))$. With the formula $F(y) = \frac{1}{2\pi^2}\int_0^\pi \int_{\mathbb{R}}((\cos(\alpha),\sin(\alpha))\bullet y - s)^{-1}(\partial_s\mathcal{R}F)(\alpha,s)\mathrm{d}s\mathrm{d}\alpha$ for inverting the Radon transform (see, for example, [14, 21]) this yields

$$\sum_{\sigma=\pm1} F_\sigma(y) = \frac{1}{2\pi^2}\int_0^\pi\int_{-1}^1 \frac{\partial_{\cos(\psi)}[\mathcal{C}_k f(\varphi,z,\alpha-\pi/2,\psi)/\sin\psi]}{y\bullet(\cos(\alpha),\sin(\alpha)) - \cos(\psi)}\mathrm{d}(\cos\psi)\mathrm{d}\alpha$$
$$= \frac{1}{2\pi^2}\int_0^\pi\int_0^\pi \frac{\partial_\psi[\mathcal{C}_k f(\varphi,z,\alpha-\pi/2,\psi)/\sin\psi]}{\cos(\psi) - (\cos(\alpha),\sin(\alpha))\bullet y}\mathrm{d}\psi\mathrm{d}\alpha.$$

Inserting the definition of F_σ yields (3.3).

By the chain rule we have

$$(\partial_w^k\mathcal{X}_0 f)(\varphi,z,v,w) = \int_0^\infty \partial_w^k f\left((\theta(\varphi),z) + r(v,w)\right)\mathrm{d}r$$
$$= \int_0^\infty \partial_z^k f\left((\theta(\varphi),z) + r(v,w)\right) r^k \mathrm{d}r = (\partial_z^k\mathcal{X}_k f)(\varphi,z,v,w)\,.$$

Together with Cauchy's formula for repeated integration we obtain

$$(\mathcal{X}_0 f)(\varphi,z,v,w) = \frac{1}{(k-1)!}\int_{-\infty}^w (w-s)^{k-1}(\partial_z^k\mathcal{X}_k f)(\varphi,z,v,s)\mathrm{d}s$$
$$= \frac{1}{(k-1)!}\int_{-\infty}^w (w-s)^{k-1}(\partial_z^k\mathcal{X}_k f)\left(\varphi,z,\frac{(v,s)}{\sqrt{\|v\|^2+s^2}}\right)\frac{\mathrm{d}s}{(\|v\|^2+s^2)^{(k+1)/2}}\,,$$

where for the second equality we used the identity $(\mathcal{X}_k f)(\varphi,z,\lambda u) = \lambda^{-k-1}(\mathcal{X}_k f)(\varphi,z,u)$ that holds for every $\lambda>0$ and $u\in\mathbb{R}^3$.

Now we take $w=0$ and $\|v\|=1$ in the last displayed equation, and make the substitution $s=\tan(\gamma)$. Then $\|v\|^2+s^2 = 1/\cos^2(\gamma)$ and $\mathrm{d}s = \mathrm{d}\gamma/\cos^2(\gamma)$. Consequently, we have

$$(\mathcal{X}_0 f)(\varphi,z,v,0) = \frac{1}{(k-1)!}\int_{-\pi/2}^0 (-\tan(\gamma))^{k-1}(\partial_z^k\mathcal{X}_k f)\left(\varphi,z,v\cos(\gamma),\sin(\gamma)\right)$$
$$\times\cos^{k-1}(\gamma)\mathrm{d}\gamma \quad \text{for } v\in\mathbb{S}^1\,,$$

which after a simple manipulation yields (3.4). ∎

The following theorem shows how to explicitly reduce the weighted conical Radon transform to the (two-dimensional) V-line transform applied in horizontal planes.

Theorem 3.3 (reduction of the conical Radon transform to the V-line transform). *Let $f\in C_c^\infty(D_1(0)\times\mathbb{R})$. Then, we have for $(\varphi,z,\psi)\in[0,2\pi)\times\mathbb{R}\times(0,\pi/2)$,*

$$\sum_{\sigma=\pm1}(\mathcal{X}_0 f)(\varphi,z,-\cos(\psi)\theta(\varphi)+\sigma\sin(\psi)\theta(\varphi)^\perp,0)\,, \tag{3.6}$$
$$= \int_0^\pi\int_0^\pi \partial_z^k\partial_\psi[\mathcal{C}_k f(\varphi,z,\beta,\psi)/\sin\psi]H_k(\beta,\psi)\mathrm{d}\psi\mathrm{d}\beta$$

with

$$H_k(\beta,\psi) := \frac{(-1)^{k-1}}{2\pi^2(k-1)!}\int_{-\pi/2}^{0}\frac{\sin^{k-1}(\gamma)\cos(\gamma)\sin(\psi)\mathrm{d}\gamma}{\cos(\psi)-(\cos(\gamma)\cos(\psi),\sin(\gamma))\bullet(\sin(\beta),\cos(\beta))}\,. \tag{3.7}$$

Proof. By Lemma 3.2 we have

$$\begin{aligned}
&\sum_{\sigma=\pm1}(\mathcal{X}_0 f)(\varphi,z,-\cos(\psi)\theta(\varphi)+\sigma\sin(\psi)\theta(\varphi)^{\perp},0) \\
&=\frac{(-1)^{k-1}}{(k-1)!}\sum_{\sigma=\pm1}\int_{-\pi/2}^{0}\sin^{k-1}(\gamma) \\
&\qquad\times(\partial_z^k\mathcal{X}_k f)\left(\varphi,z,-\cos(\gamma)\cos(\psi)\theta(\varphi)+\sigma\cos(\gamma)\sin(\psi)\theta(\varphi)^{\perp},\sin(\gamma)\right)\mathrm{d}\gamma \\
&=\frac{(-1)^{k-1}}{(k-1)!}\partial_z^k\int_{-\pi/2}^{0}\sin^{k-1}(\gamma) \\
&\qquad\times\sum_{\sigma=\pm1}(\mathcal{X}_k f)\left(\varphi,z,-\cos(\gamma)\cos(\psi)\theta(\varphi)+\sigma\cos(\gamma)\sin(\psi)\theta(\varphi)^{\perp},\sin(\gamma)\right)\mathrm{d}\gamma \\
&=\frac{(-1)^{k-1}}{2\pi^2(k-1)!}\int_{-\pi/2}^{0}\int_0^{\pi}\int_0^{\pi}\frac{\sin^{k-1}(\gamma)\cos(\gamma)\sin(\psi)\partial_z^k\partial_\psi[\mathcal{C}_k f(\varphi,z,\beta,\psi)/\sin\psi]\mathrm{d}\psi\mathrm{d}\beta\mathrm{d}\gamma}{\cos(\psi)-(-\cos(\gamma)\cos(\psi),\sin(\gamma))\bullet(-\sin(\beta),\cos(\beta))}\,.
\end{aligned} \tag{3.8}$$

Interchanging the order of integrations and using the definition of the kernel $H_k(\beta,\psi)$ yields the desired identity. ∎

Let $f\in C_c^\infty(D_1(0)\times\mathbb{R})$. For any given $z\in\mathbb{R}$ define $f_z := f(\,\cdot\,,z)$. Therefore, the V-line transform of f_z satisfies

$$\begin{aligned}
(\mathcal{V}f_z)(\varphi,\psi) &= \sum_{\sigma=\pm1}\int_0^{\infty} f(\theta(\varphi)-r(\cos(\varphi-\sigma\psi),\sin(\varphi-\sigma\psi)),z)\mathrm{d}r \\
&= \sum_{\sigma=\pm1}(\mathcal{X}_0 f)(\varphi,z,-\cos(\psi)\theta(\varphi)+\sigma\sin(\psi)\theta(\varphi)^{\perp},0) \\
&= \int_0^{\pi}\int_0^{\pi}\partial_z^k\partial_\psi[\mathcal{C}_k f(\varphi,z,\beta,\psi)/\sin\psi]H_k(\beta,\psi,\gamma)\mathrm{d}\psi\mathrm{d}\beta\,.
\end{aligned} \tag{3.9}$$

Here the second equality will then follow from the identity $-\cos(\psi)\theta(\varphi)+\sigma\sin(\psi)\theta(\varphi)^{\perp} = -(\cos(\varphi-\sigma\psi),\sin(\varphi-\sigma\psi))$ and the last equality from Theorem 3.3. Equation (3.9) shows how to recover the V-line transform $\mathcal{V}f_z$ from the conical Radon transform. By subsequently inverting the V-line transform one recovers f. In summary, we conclude the following inversion method for the conical Radon transform.

Algorithm 3.4 (inversion of the conical Radon transform, Method 1).
- Step 1: *Compute the kernel H_k defined in (3.7).*
- Step 2: *Evaluate (3.9) to recover $\mathcal{V}f_z$ from $\mathcal{C}_k f$ for every $z\in\mathbb{R}$.*
- Step 3: *For every $z\in\mathbb{R}$ recover f_z from $\mathcal{V}f_z$ by means of Algorithm 2.4.*

Theorem 3.3 also implies that the considered conical Radon transform $f \mapsto \mathcal{C}_k f$ is uniquely invertible and can be reconstructed by Algorithm 3.4. How to efficiently implement Algorithm 3.4 is a topic of future work.

Note that the data function $\mathcal{C}_k f$ has unbounded support even if the unknown function has compact support. Therefore in the actual computation the data have to be truncated for values of z outside some fixed interval of finite length. In particular, some boundaries of f that are almost vertical will become invisible, in the sense that there are no data value available that correspond to the integral over a conical surface touching the boundary. Hence one faces a so-called limited view problem. Similar to the inversion of other Radon transforms (see, for example, [2, 10, 17, 21, 22, 29]) one can expect that this introduces typical limited view artifacts which manifest in the form of smearing out of invisible boundaries.

3.2. Method 2: Reduction to the Radon transform. The second method is probably simpler than the method presented above, but only works for the cases $k = 0, 1$. It is based on a relation between the conical Radon transform and the regular three-dimensional Radon transform, that has first been derived by Smith [27]. For that purpose we use the following additional notations:

- $(\mathcal{R}f)(\omega, s) := \int_{\omega^\perp} f(s\omega + y)\mathrm{d}S(y)$ for $(\omega, s) \in \mathbb{S}^2 \times \mathbb{R}$ denotes the regular three-dimensional Radon transform of $f \in C_c^\infty(\mathbb{R}^3)$;
- $(\mathcal{H}g)(\omega, s) := \frac{1}{\pi} \int_{\mathbb{R}} g(\omega, t)\mathrm{d}t/(s - t)$ for $(\omega, s) \in \mathbb{S}^2 \times \mathbb{R}$ denotes the Hilbert transform in the second component of a function $g \in C_c^\infty(\mathbb{S}^2 \times \mathbb{R})$.

While the reduction to the three-dimensional Radon transform has already been obtained by [27], in this paper we go one step further and use this approach to formulate various explicit inversion formulas for the conical Radon transform (Theorem 3.7 and Corollary 3.8). These inversion formulas are of practical as well as theoretical use. Specifically, in this paper we derive stability estimates as a result of the explicit inversion formulas; see Theorem 3.9.

Lemma 3.5 (reduction of the conical Radon transform to the Radon transform). *Let $f \in C_c^\infty(\mathbb{R}^3)$. Then, for $(\varphi, z, \beta) \in [0, 2\pi) \times \mathbb{R} \times (0, \pi)$, we have*

$$(\mathcal{H}\partial_s \mathcal{R}f)(a(\varphi, \beta), z\cos(\beta) - \sin(\beta)) = -\frac{1}{\pi} \int_0^\pi (\mathcal{C}_0 f)(\varphi, z, \beta, \psi) \frac{\mathrm{d}\psi}{\cos(\psi)^2}, \tag{3.10}$$

$$(\mathcal{H}\mathcal{R}f)(a(\varphi, \beta), z\cos(\beta) - \sin(\beta)) = -\frac{1}{\pi} \int_0^\pi (\mathcal{C}_1 f)(\varphi, z, \beta, \psi) \frac{\mathrm{d}\psi}{\cos(\psi)}. \tag{3.11}$$

Proof. Expressing $\mathcal{C}_k$ for $k = 0, 1$ in terms of the one-dimensional delta distribution and performing several coordinate substitutions yield

$$\begin{aligned}
&\int_0^\pi \mathcal{C}_k f(\varphi, z, \beta, \psi) \cos^{k-2}(\psi)\mathrm{d}\psi \\
&\quad = \int_0^\pi \int_{\mathbb{S}^2} \int_0^\infty f\left((\theta(\varphi), z) + r\omega\right) \delta\left(a(\varphi, \beta) \bullet \omega - \cos(\psi)\right) r^k \mathrm{d}r\mathrm{d}S(\omega) \cos^{k-2}(\psi)\mathrm{d}(\cos(\psi)) \\
&\quad = \int_{\mathbb{S}^2} \int_0^\infty f\left((\theta(\varphi), z) + r\omega\right) \left(a(\varphi, \beta) \bullet \omega\right)^{k-2} r^k \mathrm{d}r\mathrm{d}S(\omega)
\end{aligned}$$

$$
\begin{aligned}
&= \int_{\mathbb{R}^3} f\left((\theta(\varphi), z) + x\right)(a(\varphi,\beta)\bullet x)^{k-2}\mathrm{d}x \\
&= \int_{\mathbb{R}^3} f(x)(a(\varphi,\beta)\bullet x - a(\varphi,\beta)\bullet(\theta(\varphi), z))^{k-2}\mathrm{d}x \\
&= \int_{\mathbb{R}}\int_{a(\varphi,\beta)^\perp} f(sa(\varphi,\beta)+y)(s+\sin(\beta)-z\cos(\beta))^{k-2}\mathrm{d}y\mathrm{d}s \\
&= \int_{\mathbb{R}} (\mathcal{R}f)(a(\varphi,\beta),s)(s+\sin(\beta)-z\cos(\beta))^{k-2}\mathrm{d}s.
\end{aligned}
$$

Here the third equality follows after introducing spherical coordinates $x \leftarrow r\omega$, the fourth equality follows after the change of variables $x \leftarrow (\theta(\varphi), z) + x$, the fifth equality follows after the substitution $x \leftarrow sa(\varphi,\beta)+y$, and the last equality follows from the definition of the Radon transform. Now, the definition of the Hilbert transform and performing one integration by parts in the case $k = 0$ yield (3.10), (3.11). ∎

Using Lemma 3.5 we can recover $\mathcal{H}\partial_s^{1-k}\mathcal{R}f$ from the conical Radon transform. By applying the inverse Hilbert transform and the inverse Radon transform afterwards, one then recovers the original function. This yields the following reconstruction method.

Algorithm 3.6 (inversion of the conical Radon transform for $k = 0, 1$, Method 2).
- Step 1: *Recover* $\mathcal{H}\partial_s^{1-k}\mathcal{R}f$ *from* $\mathcal{C}_k f$ *by evaluating* (3.10) *or* (3.11).
- Step 2: *Recover* $\partial_s^{1-k}\mathcal{R}f$ *from* $\mathcal{H}\partial_s^{1-k}\mathcal{R}f$ *by applying the inverse Hilbert transform.*
- Step 3: *Recover* f *from* $\partial_s^{1-k}\mathcal{R}f$ *by applying the inverse Radon transform.*

While Algorithm 3.6 can efficiently be implemented, one can combine three steps to obtain an explicit inversion formula. Such inversion formulas are also useful for theoretical investigations. By using the standard filtered backprojection-type inversion formulas for the Radon transform (see, for example, [14, 21])

$$
f(x) = -\frac{1}{8\pi^2}\Delta_x \int_{\mathbb{S}^2} \mathcal{R}f(\omega, \omega\bullet x)\mathrm{d}S(\omega)\,, \tag{3.12}
$$

$$
f(x) = -\frac{1}{8\pi^2}\int_{\mathbb{S}^2} \partial_t^2\mathcal{R}f(\omega, \omega\bullet x)\mathrm{d}S(\omega)\,, \tag{3.13}
$$

Lemma 3.5 yields the following result.

Theorem 3.7. *For* $f \in C^\infty(D_1(0)\times\mathbb{R})$ *we have*

$$
f(x) = -\frac{1}{8\pi^4}\int_{\mathbb{S}^2}\int_{\mathbb{R}}\int_0^\pi \frac{(\partial_z^2\mathcal{C}_k f)(\varphi, z, \beta, \psi)\cos^{-k}(\beta)\mathrm{d}\psi\mathrm{d}z\mathrm{d}S(a(\varphi,\beta))}{(x\bullet a(\varphi,\beta) - z\cos(\beta)+\sin(\beta))\cos^{2-k}(\psi)} \qquad \text{for } k\in\{0,1\}\,, \tag{3.14}
$$

$$
f(x) = -\frac{1}{8\pi^4}\Delta_x\int_{\mathbb{S}^2}\int_{\mathbb{R}}\int_0^\pi \frac{\mathcal{C}_1 f(\varphi, z, \beta, \psi)\cos(\beta)\mathrm{d}\psi\mathrm{d}z\mathrm{d}S(a(\varphi,\beta))}{(x\bullet a(\varphi,\beta) - z\cos(\beta)+\sin(\beta))\cos(\psi)} \qquad \text{for } k = 0\,. \tag{3.15}
$$

Proof. Since $\mathcal{H}\mathcal{H}g = -g$, we have

$$\begin{aligned}\partial_s^{1-k}\mathcal{R}f(a(\varphi,\beta),s) &= -\partial_s^{1-k}(\mathcal{H}\mathcal{H}\mathcal{R}f)(a(\varphi,\beta),s)\\ &= \frac{(-1)^k}{\pi}\int_{\mathbb{R}}\frac{\mathcal{H}\mathcal{R}f(a(\varphi,\beta),z\cos(\beta)-\sin(\beta))\cos(\beta)\mathrm{d}z}{(s-z\cos(\beta)+\sin(\beta))^{2-k}}\\ &= -\frac{1}{\pi}\int_{\mathbb{R}}\frac{\partial_z^{1-k}\mathcal{H}\mathcal{R}f(a(\varphi,\beta),z\cos(\beta)-\sin(\beta))\cos^k(\beta)\mathrm{d}z}{s-z\cos(\beta)+\sin(\beta)}\\ &= \frac{1}{\pi^2}\int_{\mathbb{R}}\int_0^\pi\frac{\partial_z^{1-k}\mathcal{C}_kf(\varphi,z,\beta,\psi)\cos(\beta)\mathrm{d}\psi\mathrm{d}z}{(s-z\cos(\beta)+\sin(\beta))\cos^{2-k}(\psi)}\,.\end{aligned}$$

Together with (3.12) this yields (3.15) for $k=1$. Further, integration by parts shows

$$\begin{aligned}&(\partial_s^2\mathcal{R}f)(a(\varphi,\beta),t)\\ &= (\partial_s^{1+k}\partial_s^{1-k}\mathcal{R}f)(a(\varphi,\beta),t)\\ &= \frac{(-1)^{k+1}(k+1)!}{\pi^2}\int_{\mathbb{R}}\int_0^\pi\frac{(\partial_z^{1-k}\mathcal{C}_kf)(\varphi,z,\beta,\psi)\cos(\beta)\mathrm{d}\psi\mathrm{d}z}{(s-z\cos(\beta)+\sin(\beta))^{2+k}\cos^{2-k}(\psi)}\\ &= \frac{(-1)^{k+1}}{\pi^2}\int_{\mathbb{R}}\int_0^\pi\partial_z^{1+k}\left[\frac{1}{s-z\cos(\beta)+\sin(\beta)}\right](\partial_z^{1-k}\mathcal{C}_kf)(\varphi,z,\beta,\psi)\cos^{-k}(\beta)\frac{\mathrm{d}\psi\mathrm{d}z}{\cos^{2-k}(\psi)}\\ &= \frac{1}{\pi^2}\int_{\mathbb{R}}\int_0^\pi\frac{(\partial_z^2\mathcal{C}_kf)(\varphi,z,\beta,\psi)\cos^{-k}(\beta)}{(s-z\cos(\beta)+\sin(\beta))\cos^{2-k}(\psi)}\mathrm{d}\psi\mathrm{d}z\,,\end{aligned}$$

which together with (3.13) yields (3.14). ∎

The inversion formulas (3.14) for $k=0$ and (3.15) for $k=1$ can further be rewritten in terms of the conical backprojection operator $\mathcal{C}_k^\sharp g$ that is defined by

$$\begin{aligned}(3.16)\quad \mathcal{C}_k^\sharp g(x) = &\int_0^\pi\int_0^\pi\int_{\mathbb{R}}\int_0^{2\pi} g(\varphi,z,\beta,\psi)\|x-(\theta(\varphi),z)\|^{k-1}\\ &\times\delta(a(\varphi,\beta)\bullet x - z\cos(\beta)+\sin(\beta)-\|x-(\theta(\varphi),z)\|\cos(\psi))\sin(\psi)\mathrm{d}\varphi\mathrm{d}z\mathrm{d}\beta\mathrm{d}\psi\end{aligned}$$

for $g\in C^\infty([0,2\pi)\times\mathbb{R}\times(0,\pi)^2)$ and $x\in\mathbb{R}^3$. As shown in Appendix A.1, the operator $\mathcal{C}_k^\sharp$ is the (formal) L^2-adjoint of $\mathcal{C}_k$.

Corollary 3.8. *Let $f\in C^\infty(D_1(0)\times\mathbb{R})$. Then we have for $x\in\mathbb{R}^3$,*

$$(3.17)\qquad f(x) = \frac{(-1)^k}{8\pi^4}\Delta_x^k\mathcal{C}_k^\sharp\left[\int_0^\pi\frac{\partial_z^{1-k}\mathcal{C}_kf(\varphi,z,\beta,\psi')\cos(\beta)\sin(\beta)\mathrm{d}\psi'}{\cos^{2-k}(\psi)\cos^{2-k}(\psi')}\right](x).$$

Proof. See Appendix A.2 ∎

Using Corollary 3.8, we can easily derive a stability estimate for the conical Radon transform. For that purpose we denote by $\mathcal{F}f$ the Fourier transform of f and set

$$\begin{aligned}\|f\|_{-1}^2 &= \int_{\mathbb{R}^3}|\mathcal{F}f(\xi)|^2(\|\xi\|^2+1)^{-1}\mathrm{d}\xi,\\ \|\mathcal{C}_kf\|^2 &= \int_0^\pi\int_{\mathbb{R}}\int_0^{2\pi}\int_0^\pi\left|\frac{\mathcal{C}_kf(\varphi,z,\beta,\psi)}{\cos^{2-k}(\psi)}\right|^2\cos(\beta)\sin(\beta)\mathrm{d}\psi\mathrm{d}\varphi\mathrm{d}z\mathrm{d}\beta\,,\\ \|\mathcal{C}_kf\|_1^2 &= \|\mathcal{C}_kf\|^2+\|\partial_z\mathcal{C}_kf\|^2\,.\end{aligned}$$

Theorem 3.9. *For $f \in C_c^\infty(D_1(0)\times\mathbb{R})$ we have $\|f\|_{-1} \le \|\mathcal{C}_1 f\|$ and $\|f\| \le \pi/2\|\mathcal{C}_0 f\|_1$.*

Proof. By Corollary 3.8 with $k=1$ we have

$$
\begin{aligned}
(3.18)\quad \|f\|_{-1}^2 &\le \int_{\mathbb{R}^3} |\mathcal{F}f(\xi)|^2 \,\|\xi\|^{-2}\,\mathrm{d}\xi \\
&= -(2\pi)^3 \int_{\mathbb{R}^3} f(x)\Delta_x^{-1} f(x)\mathrm{d}x \\
&= \frac{1}{\pi}\int_{\mathbb{R}^3} f(x)\mathcal{C}_1^\sharp\left[\int_0^\pi \frac{\mathcal{C}_1 f(\varphi,z,\beta,\psi')\cos(\beta)\sin(\beta)\mathrm{d}\psi'}{\cos(\psi)\cos(\psi')}\right](x)\mathrm{d}x \\
&= \frac{1}{\pi}\int_0^\pi\int_0^\pi\int_{\mathbb{R}}\int_0^{2\pi} \mathcal{C}_1 f(\varphi,z,\beta,\psi)\int_0^\pi \frac{\mathcal{C}_1 f(\varphi,z,\beta,\psi')\cos(\beta)\sin(\beta)\mathrm{d}\psi'}{\cos(\psi)\cos(\psi')}\mathrm{d}\varphi\mathrm{d}z\mathrm{d}\beta d\psi \\
&= \frac{1}{\pi}\int_0^\pi\int_{\mathbb{R}}\int_0^{2\pi}\left(\int_0^\pi \frac{\mathcal{C}_1 f(\varphi,z,\beta,\psi)}{\cos(\psi)}\mathrm{d}\psi\right)^2 \cos(\beta)\sin(\beta)\mathrm{d}\varphi\mathrm{d}z\mathrm{d}\beta\,,
\end{aligned}
$$

where the third equality holds because $\mathcal{C}_1^\sharp$ is the L^2-adjoint of $\mathcal{C}_1$. Applying Jensen's inequality to the inner integral completes our proof.

Now suppose $k=0$. Similarly to (3.18) we have

$$
\begin{aligned}
\|f\|^2 &= \frac{1}{\pi}\int_0^\pi\int_{\mathbb{R}}\int_0^{2\pi}\left(\int_0^\pi \frac{\mathcal{C}_0 f(\varphi,z,\beta,\psi)}{\cos^2(\psi)}\mathrm{d}\psi\right) \\
&\qquad\times\left(\int_0^\pi \frac{\partial_z\mathcal{C}_0 f(\varphi,z,\beta,\psi)}{\cos^2(\psi)}\mathrm{d}\psi\right)\cos(\beta)\sin(\beta)\mathrm{d}\varphi\mathrm{d}z\mathrm{d}\beta \\
&\le \frac{1}{\pi}\left(\int_0^\pi\int_{\mathbb{R}}\int_0^{2\pi}\left(\int_0^\pi \frac{\mathcal{C}_0 f(\varphi,z,\beta,\psi)}{\cos^2(\psi)}\mathrm{d}\psi\right)^2\cos(\beta)\sin(\beta)\mathrm{d}\varphi\mathrm{d}z\mathrm{d}\beta\right)^{1/2} \\
&\qquad\times\left(\int_0^\pi\int_{\mathbb{R}}\int_0^{2\pi}\left(\int_0^\pi \frac{\partial_z\mathcal{C}_0 f(\varphi,z,\beta,\psi)}{\cos^2(\psi)}\mathrm{d}\psi\right)^2\cos(\beta)\sin(\beta)\mathrm{d}\varphi\mathrm{d}z\mathrm{d}\beta\right)^{1/2},
\end{aligned}
$$

where in the second line we used the Cauchy–Schwarz inequality. By Jensen's inequality, we have

$$
\begin{aligned}
\|f\|^2 &\le \pi\left(\int_0^\pi\int_{\mathbb{R}}\int_0^{2\pi}\int_0^\pi \left|\frac{\mathcal{C}_0 f(\varphi,z,\beta,\psi)}{\cos^2(\psi)}\right|^2 \mathrm{d}\psi\cos(\beta)\sin(\beta)\mathrm{d}\varphi\mathrm{d}z\mathrm{d}\beta\right)^{1/2} \\
&\qquad\times\left(\int_0^\pi\int_{\mathbb{R}}\int_0^{2\pi}\int_0^\pi \left|\frac{\partial_z\mathcal{C}_0 f(\varphi,z,\beta,\psi)}{\cos^2(\psi)}\right|^2 \mathrm{d}\psi\cos(\beta)\sin(\beta)\mathrm{d}\varphi\mathrm{d}z\mathrm{d}\beta\right)^{1/2} \\
&\le \frac{\pi}{2}\left(\int_0^\pi\int_{\mathbb{R}}\int_0^{2\pi}\int_0^\pi \left|\frac{\mathcal{C}_0 f(\varphi,z,\beta,\psi)}{\cos^2(\psi)}\right|^2 \mathrm{d}\psi\cos(\beta)\sin(\beta)\mathrm{d}\varphi\mathrm{d}z\mathrm{d}\beta\right) \\
&\qquad+\frac{\pi}{2}\left(\int_0^\pi\int_{\mathbb{R}}\int_0^{2\pi}\int_0^\pi \left|\frac{\partial_z\mathcal{C}_0 f(\varphi,z,\beta,\psi)}{\cos^2(\psi)}\right|^2 \mathrm{d}\psi\cos(\beta)\sin(\beta)\mathrm{d}\varphi\mathrm{d}z\mathrm{d}\beta\right). \qquad \blacksquare
\end{aligned}
$$

4. Discussion and outlook. In this paper we studied the weighted conical Radon $\mathcal{C}_k$ that integrates a function over all cones having their vertex on a circular cylinder and central axis pointing to the symmetry axis of the cylinder. We presented two explicit reconstruction procedures (see Algorithms 3.4 and 3.6). The first approach is based on reducing $\mathcal{C}_k$ to the V-line transform with vertices on the circle. For the V-line transform we derived an explicit inversion formula based on Fourier series expansion and a corresponding efficient discrete reconstruction algorithm. The second approach is based on reducing $\mathcal{C}_k$ to the classical Radon transform as first proposed by Smith [27]. Finally, we derived novel Sobolev stability estimates for the weighted conical Radon $\mathcal{C}_k$. We expect also that Algorithms 3.4 and 3.6 for inverting $\mathcal{C}_k$ can be implemented efficiently and future work will be done to numerically implement these reconstruction methods. We intend to compare these methods with iterative procedures in terms of computation time and image quality for realistically simulated data.

The conical Radon transform is motivated from its application to image reconstruction in emission tomography using Compton cameras. The family of cones of integration we considered in this paper depends on four parameters, whereas the function to be recovered only depends on three parameters. Therefore, the reconstruction problem for the studied transform is overdetermined. Because of the low number of photons typically emitted in emission tomography, the redundancy in the data is actually a positive property of Compton camera imaging. Moreover as the considered problem is overdetermined, no exact solution exists in the case of noisy data. Linear reconstruction procedures such as Algorithms 3.4 or 3.6 can be thought of as being applied separately to the exact data and the noise. In particular, some part of the noise that is outside the range of the forward operator will be eliminated by the reconstruction algorithm. Currently it is not clear which of the two algorithms performs better with respect to this issue. However, Algorithm 3.4 as well as Algorithm 3.6 inherently contain some form of averaging and therefore one can expect partial cancelation effects for the case of oscillating noise. Investigating such issues more closely will be the subject of future research.

Despite the redundancy having a positive effect for noise reduction, it is also of interest from a theoretical as well as a practical point of view to study uniqueness and stability of reconstruction for nonoverdetermined sets of conical integrals with vertices on a fixed surface. Not much is known in such a direction. The best studied instance of such a nonredundant transform uses integrals over cones with vertices on a plane and symmetry axis orthogonal to that plane. In this case uniqueness results and a Fourier slice identity [7, 12, 23] as well as stable inversion formulas and Sobolev space estimates are available [12, 19]. Another instance where some results are available is the case where the cones of integration have vertices on a sphere and symmetry axis orthogonal to the sphere. In this case uniqueness and a computationally efficient inversion procedure using spherical harmonics have been derived in [25]. However neither an explicit inversion formula nor stability estimates are known in this case. Opposed to the planar and spherical analogs, the conical Radon transform with vertices located on a cylinder and symmetry axes orthogonal to the cylinder has not been studied so far. In particular, it is currently not known whether such a transform yields unique reconstruction or a (stable and computationally efficient) reconstruction procedure. Such investigations are interesting lines of future research.

Appendix A. Proofs.

A.1. Formal L^2-adjoint of $\mathcal{C}_k$. We have

$$\begin{aligned}
&\int_0^\pi \int_0^\pi \int_{\mathbb{R}} \int_0^{2\pi} \mathcal{C}_k f(\varphi,z,\beta,\psi) g(\varphi,z,\beta,\psi) \mathrm{d}\varphi \mathrm{d}z \mathrm{d}\beta \mathrm{d}\psi \\
&= \int_0^\pi \int_0^\pi \int_{\mathbb{R}} \int_0^{2\pi} \int_{\mathbb{R}^3} f((\theta(\varphi),z)+x) \delta(a(\varphi,\beta)\bullet x - \|x\|\cos(\psi)) \\
&\qquad \times g(\varphi,z,\beta,\psi) \frac{\sin(\psi)\mathrm{d}x}{\|x\|^{1-k}} \mathrm{d}\varphi \mathrm{d}z \mathrm{d}\beta \mathrm{d}\psi \\
&= \int_{\mathbb{R}^3} \int_0^\pi \int_0^\pi \int_{\mathbb{R}} \int_0^{2\pi} f(x) g(\varphi,z,\beta,\psi) \|x-(\theta(\varphi),z)\|^{k-1} \\
&\qquad \times \delta(a(\varphi,\beta)\bullet x - z\cos(\beta) + \sin(\beta) - \|x-(\theta(\varphi),z)\|\cos(\psi)) \sin(\psi) \mathrm{d}\varphi \mathrm{d}z \mathrm{d}\beta \mathrm{d}\psi \mathrm{d}x \\
&= \int_{\mathbb{R}^3} f(x) \mathcal{C}_k^\sharp g(x) \mathrm{d}x\,.
\end{aligned}$$

Here for the first and second equalities, we made use of the change of variables $x \leftarrow r\omega$ and $x \leftarrow (\theta(\varphi),z)+x$, respectively.

A.2. Proof of Corollary 3.8. It is enough to show that for fixed $x \in \mathbb{R}^3$ and $k = 0, 1$, we have

$$\begin{aligned}
(\mathrm{A.1}) \quad &\mathcal{C}_k^\sharp \left[\int_0^\pi \frac{\partial_z^{1-k} g(\varphi,z,\beta,\psi') \cos(\beta)\sin(\beta)\mathrm{d}\psi'}{\cos^{2-k}(\psi)\cos^{2-k}(\psi')} \right](x) \\
&\qquad = (-1)^{k+1} \int_{\mathbb{S}^2} \int_{\mathbb{R}} \int_0^\pi \frac{\partial_z^{2-2k} g(\varphi,z,\beta,\psi)\cos^k(\beta)\mathrm{d}\psi \mathrm{d}z \mathrm{d}S(a(\varphi,\beta))}{(a(\varphi,\beta)\bullet x - z\cos(\beta)+\sin(\beta))\cos^{2-k}(\psi)}\,.
\end{aligned}$$

By the definition of $\mathcal{C}_k^\sharp$ and the homogeneity of the one-dimensional delta distribution, the left-hand side of (A.1) becomes

$$\begin{aligned}
&\int_0^\pi \int_{\mathbb{R}} \int_0^{2\pi} \int_0^\pi \int_0^\pi \frac{\partial_z^{1-k} g(\varphi,z,\beta,\psi')\cos(\beta)\sin(\beta)}{\cos^{2-k}(\psi)\cos^{2-k}(\psi')\|x-(\theta(\varphi),z)\|^{2-k}} \\
&\qquad \times \delta\left(\frac{a(\varphi,\beta)\bullet x - z\cos(\beta)+\sin(\beta)}{\|x-(\theta(\varphi),z)\|} - \cos(\psi) \right) \sin(\psi)\mathrm{d}\psi' \mathrm{d}\psi \mathrm{d}\varphi \mathrm{d}z \mathrm{d}\beta \\
&= \int_0^\pi \int_{\mathbb{R}} \int_0^{2\pi} \int_0^\pi \frac{\partial_z^{1-k} g(\varphi,z,\beta,\psi')\cos(\beta)\sin(\beta)\mathrm{d}\psi' \mathrm{d}\varphi \mathrm{d}z \mathrm{d}\beta}{(a(\varphi,\beta)\bullet x - z\cos(\beta)+\sin(\beta))^{2-k}\cos^{2-k}(\psi')}\,.
\end{aligned}$$

Now the surface measure of the sphere is $\sin(\beta)\mathrm{d}\varphi\mathrm{d}\beta$ when φ and β are the azimuthal and polar angles, respectively. Thus we have

$$\begin{aligned}
&\mathcal{C}_k^\sharp \left[\int_0^\pi \frac{\partial_z^{1-k} g(\varphi,z,\beta,\psi')\cos(\beta)\sin(\beta)\mathrm{d}\psi'}{\cos^{2-k}(\psi)\cos^{2-k}(\psi')} \right](x) \\
&\qquad = \int_{\mathbb{S}^2} \int_{\mathbb{R}} \int_0^\pi \frac{\partial_z^{1-k} g(\varphi,z,\beta,\psi)\cos(\beta)\mathrm{d}\psi \mathrm{d}z \mathrm{d}S(\varphi,\beta)}{(a(\varphi,\beta)\bullet x - z\cos(\beta)+\sin(\beta))^{2-k}\cos^{2-k}(\psi)}\,.
\end{aligned}$$

If $k = 1$, the proof is done. If $k = 0$, then integration by parts completes the proof.

Appendix B. Generalization to higher dimension.

In this section we generalize the results for the conical Radon transform presented in subsection 3.2 to a general dimension. For the following, let $n \geq 3$.

Definition B.1 (the conical Radon transform on the cylinder in $\mathbb{R}^n$). *Let $f \in C_c^\infty(B_1(0) \times \mathbb{R})$. We define the* conical Radon transform in $\mathbb{R}^n$ $\mathcal{C}f\colon \mathbb{S}^{n-2} \times \mathbb{R} \times (0,\pi)^2 \to \mathbb{R}$ *by*

$$\mathcal{C}f(\theta, z, \beta, \psi) := \sin(\psi) \int_{\mathbb{S}^{n-1}} \int_0^\infty f((\theta, z) + r\omega) r^{n-2} \delta(\omega \cdot a(\theta,\beta) - \cos(\psi)) \mathrm{d}r \mathrm{d}S(\omega)\,,$$

where $a(\theta,\beta) := (-\theta\sin(\beta), \cos(\beta))$.

As in the three-dimensional case the formal L^2-adjoint of $\mathcal{C}$ is given by

$$\begin{aligned}(\mathrm{B}.1)\quad \mathcal{C}^\sharp g(x) = \int_0^\pi \int_0^\pi \int_{\mathbb{R}} \int_{\mathbb{S}^{n-2}} & g(\theta, z, \beta, \psi) \\ & \times \delta(x \cdot a(\theta,\beta) - z\cos(\beta) + \sin(\beta) - \|x - (\theta, z)\| \cos(\psi)) \sin(\psi) \mathrm{d}S(\theta) \mathrm{d}z \mathrm{d}\beta \mathrm{d}\psi\,.\end{aligned}$$

We further use the following notations:

- $\mathcal{R}f(\omega, s)$ for the regular n-dimensional Radon transform;
- $\mathcal{F}f(\xi)$ for the n-dimensional Fourier transform;
- $(-\Delta_x)^{(n-1)/2} f := \mathcal{F}^{-1}(\|\xi\|^{n-1} \mathcal{F}f)$ for the fractional Laplacian;
- $\|f\|^2_{-(n-1)/2} := \int_{\mathbb{R}^n} |\mathcal{F}f(\xi)|^2 (\|\xi\|^2 + 1)^{-(n-1)/2} \mathrm{d}\xi$;
- $\|\mathcal{C}f\|^2 := \int_0^\pi \int_{\mathbb{R}} \int_{\mathbb{S}^{n-2}} \int_0^\pi |\mathcal{C}f(\theta, z, \beta, \psi)/\cos(\psi)|^2 \cos(\beta)\sin(\beta)\, \mathrm{d}\psi \mathrm{d}S(\theta) \mathrm{d}z \mathrm{d}\beta$.

Similarly to the three-dimensional case one then has the following results.

Theorem B.2. *For any $f \in C_c^\infty(B_1(0) \times \mathbb{R})$ the following hold:*
Relation to Radon transform: For every $(\theta, \beta, t) \in \mathbb{S}^{n-1} \times (0,\pi) \times \mathbb{R}$,

$$\mathcal{R}f(a(\theta,\beta), t) = \frac{1}{\pi^2} \int_{\mathbb{R}} \int_0^\pi \frac{\mathcal{C}f(\theta, z, \beta, \psi) \cos(\beta) \mathrm{d}\psi \mathrm{d}z}{(t - z\cos(\beta) + \sin(\beta)) \cos(\psi)}\,.$$

Inversion formulas: For every $x \in \mathbb{R}^n$,

$$(\mathrm{B}.2)\qquad f(x) = \frac{1}{\pi(2\pi)^n} \Delta_x^{(n-1)/2} \int_0^\pi \int_{\mathbb{S}^{n-2}} \int_{\mathbb{R}} \int_0^\pi \frac{\mathcal{C}f(\theta, z, \beta, \psi) \cos(\beta)\sin(\beta) \mathrm{d}\psi \mathrm{d}z \mathrm{d}S(\theta) \mathrm{d}\beta}{(x \cdot a(\theta,\beta) - z\cos(\beta) + \sin(\beta)) \cos(\psi)}\,,$$

$$(\mathrm{B}.3)\qquad f(x) = \frac{1}{\pi(2\pi)^n} \Delta_x^{(n-1)/2} \mathcal{C}^\sharp \left[\int_0^\pi \frac{\mathcal{C}f(\theta, z, \beta, \psi') \cos(\beta)\sin(\beta) \mathrm{d}\psi'}{\cos(\psi)\cos(\psi')} \right](x)\,.$$

Stability estimate: $\|f\|_{-(n-1)/2} \leq \|\mathcal{C}f\|$.

Proof. The proof is analogous to the three-dimensional case and is therefore omitted. ∎

Finally we note that similarly to the three-dimensional case one could also derive inversion formulas and stability estimates for the weighted conical Radon transform.

Acknowledgment. SM thanks the University of Innsbruck for its hospitality during his visit.

REFERENCES

[1] M. Allmaras, D. Darrow, Y. Hristova, G. Kanschat, and P. Kuchment, *Detecting small low emission radiating sources*, Inverse Probl. Imaging, 7 (2013), pp. 47–79.

[2] L. L. Barannyk, J. Frikel, and L. V. Nguyen, *On artifacts in limited data spherical radon transform: Curved observation surface*, Inverse Problems., 32 (2015).

[3] R. Basko, G. L. Zeng, and G. T. Gullberg, *Analytical reconstruction formula for one-dimensional Compton camera*, IEEE Trans. Nucl. Sci., 44 (1997), pp. 1342–1346.

[4] R. Basko, G. L. Zeng, and G. T. Gullberg, *Application of spherical harmonics to image reconstruction for the Compton camera*, Phys. Med. Biol., 43 (1998), pp. 887–894.

[5] A. M. Cormack, *Representation of a function by its line integrals, with some radiological applications*, J. Appl. Phys., 34 (1963), pp. 2722–2727.

[6] A. M. Cormack, *Radon's problem-old and new*, in Inverse Problems, AMS, Providence, RI, SIAM-AMS Proc. 14, 1984, pp. 33–39.

[7] M. J. Cree and P. J. Bones, *Towards direct reconstruction from a gamma camera based on Compton scattering*, IEEE Trans. Med. Imaging., 13 (1994), pp. 398–407.

[8] D. B. Everett, J. S. Fleming, R. W. Todd, and J. M. Nightingale, *Gamma-radiation imaging system based on the Compton effect*, Proc. IEEE, 124 (1977), pp. 995–1000.

[9] L. Florescu, J. C. Schotland, and V. A. Markel, *Single-scattering optical tomography*, Phys. Rev. E(3), 79 (2009), 036607.

[10] J. Frikel and E. T. Quinto, *Artifacts in incomplete data tomography with applications to photoacoustic tomography and sonar*, SIAM J. Appl. Math., 75 (2015), pp. 703–725.

[11] R. Gouia-Zarrad and G. Ambartsoumian, *Exact inversion of the conical Radon transform with a fixed opening angle*, Inverse Problems, 30 (2014), 045007.

[12] M. Haltmeier, *Exact reconstruction formulas for a Radon transform over cones*, Inverse Problems, 30 (2014), p. 035001.

[13] E. W. Hansen, *Circular harmonic image reconstruction: Experiments*, Appl. Opt., 20 (1981), pp. 2266–2274.

[14] S. Helgason, *The Radon Transform*, 2nd. ed., Progr. Math., Birkhäuser, Boston, 1999.

[15] C. Jung and S. Moon, *Inversion formulas for cone transforms arising in application of Compton cameras*, Inverse Problems, 31 (2015), 015006.

[16] C.-Y. Jung and S. Moon, *Exact inversion of the cone transform arising in an application of a Compton camera consisting of line detectors*, SIAM J. Imaging Sci., 9 (2016), pp. 520–536.

[17] P. Kuchment, *The Radon Transform and Medical Imaging*, CBMS-NSF Regional Conf. Ser. in Appl. Math., 85, SIAM, Philadelphia, 2014.

[18] J. W. LeBlanc, N. H. Clinthorne, C. Hua, W. L. Rogers, D. K. Wehe, and S. J. Wilderman, *A compton camera for nuclear medicine applications using* $113mLn1$, Nucl. Instr. Meth. Phys. Res., 422 (1999), pp. 735–739.

[19] S. Moon, *On the determination of a function from its conical Radon transform with a fixed central axis*, SIAM J. Math. Anal., 48 (2016), pp. 1833–1847.

[20] M. Morvidone, M. K. Nguyen, T. T. Truong, and H. Zaidi, *On the V-line Radon transform and its imaging applications*, Int. J. Biomed. Imaging, 2010 (2010), 208179.

[21] F. Natterer, *The Mathematics of Computerized Tomography*, Classics Appl. Math. 32, SIAM, Philadelphia, 2001.

[22] L. V. Nguyen, *How strong are streak artifacts in limited angle computed tomography?*, Inverse Problems, 31 (2015), 055003.

[23] M. K. Nguyen, T. T. Truong, and P. Grangeat, *Radon transforms on a class of cones with fixed axis direction*, J. Phys. A, 38 (2005), pp. 8003–8015.

[24] R. M. Perry, *Reconstructing a function by circular harmonic analysis of line integrals*, in Image Processing for 2-D and 3-D Reconstruction from Projections: Theory and Practice in Medicine and the Physical Sciences, Digest of Technical Papers, Stanford, California, 1975.

[25] D. Schiefeneder and M. Haltmeier, *The Radon transform over cones with vertices on the sphere and orthogonal axes*. Preprint, arXiv:1606.03486, 2016.

[26] M. Singh, *An electronically collimated gamma camera for single photon emission computed tomography. part* I*: Theoretical considerations and design criteria*, Med. Phys., 10 (1983), pp. 421–427.
[27] B. Smith, *Reconstruction methods and completeness conditions for two Compton data models*, J. Opt. Soc. Amer. A, 22 (2005), pp. 445–459.
[28] B. Smith, *Line-reconstruction from Compton cameras: Data sets and a camera design*, Opt. Eng., 50 (2011), 053204.
[29] P. Stefanov and G. Uhlmann, *Is a curved flight path in SAR better than a straight one?*, SIAM J. Appl. Math., 73 (2013), pp. 1596–1612.
[30] F. Terzioglu, *Some inversion formulas for the cone transform*, Inverse Problems, 31 (2015), 115010.
[31] R. W. Todd, J. M. Nightingale, and D. B. Everett, *A proposed gamma camera*, Nature, 251 (1974), pp. 132–134.
[32] T. T. Truong and M. K. Nguyen, *On new V-line Radon transforms in* $\mathbb{R}^2$ *and their inversion*, J. Phys. A, 44 (2011), 075206.
[33] M. Wernick and J. N. Aarsvold, *Emission tomography: The fundamentals of PET and SPECT*, Academic Press, Boston, 2004.